Biomedical Optics EXPRESS

Gene transfection efficacy assessment of human cervical cancer cells using dual-mode fluorescence microendoscopy

Jaepyeong Cha,[1,*] Jing Zhang,[2] Saumya Gurbani,[1,3], Gyeong Woo Cheon,[1] Min Li,[2] and Jin U. Kang[1]

[1]*Department of Electrical and Computer Engineering, Johns Hopkins University, 3400 North Charles Street, Baltimore, MD 21218, USA*

[2]*Department of Neuroscience, School of Medicine, Johns Hopkins University, 733 North Broadway, Baltimore, MD 21205, USA*

[3]*Department of Biomedical Engineering, Johns Hopkins University, 3400 North Charles Street, Baltimore, MD 21218, USA*

**jcha8@jhu.edu*

Abstract: We report a novel approach to quantitatively assess gene transfection efficacy using dual-modality microendoscopy that can simultaneously monitor both laser scanning reflectance and fluorescence imaging. The system uses a 500-μm-diameter coherent fiber bundle and permits 3.5-μm lateral resolution. Both reflectance and fluorescence images obtained from two silicon avalanche photodetectors are displaying at 1 Hz and processed automatically to calculate gene transfection efficiency (the ratio of fluorescent cells among the total cells). To validate the system performance we examined the expression of cyan fluorescent protein using human cervical cancer cells (HeLa) in four commercially available reagents. The result was compared with that using a high-resolution bench-top microscope.

OCIS codes: (060.2350) Fiber optics imaging; (170.2520) Fluorescence microscopy; (170.2150) Endoscopic imaging.

References and links

1. M. Schiffman, P. E. Castle, J. Jeronimo, A. C. Rodriguez, and S. Wacholder, "Human papillomavirus and cervical cancer," Lancet **370**(9590), 890–907 (2007).
2. National Cancer Institute, "Cervical cancer treatment (PDQ®)," http://www.cancer.gov/cancertopics/pdq/treatment/cervical/patient/.
3. G. M. Rubanyi, "The future of human gene therapy," Mol. Aspects Med. **22**(3), 113–142 (2001).
4. D. Cross and J. K. Burmester, "Gene therapy for cancer treatment: past, present and future," Clin. Med. Res. **4**(3), 218–227 (2006).
5. D. Stone, A. David, F. Bolognani, P. R. Lowenstein, and M. G. Castro, "Viral vectors for gene delivery and gene therapy within the endocrine system," J. Endocrinol. **164**(2), 103–118 (2000).
6. D. A. Balazs and W. T. Godbey, "Liposomes for use in gene delivery," J. Drug Deliv. **2011**, 326497 (2011).
7. T. Misteli and D. L. Spector, "Applications of the green fluorescent protein in cell biology and biotechnology," Nat. Biotechnol. **15**(10), 961–964 (1997).
8. T. D. Wang and J. Van Dam, "Optical biopsy: a new frontier in endoscopic detection and diagnosis," Clin. Gastroenterol. Hepatol. **2**(9), 744–753 (2004).
9. C. Liang, M. R. Descour, K.-B. Sung, and R. Richards-Kortum, "Fiber confocal reflectance microscope (FCRM) for in-vivo imaging," Opt. Express **9**(13), 821–830 (2001).
10. K. B. Sung, C. Liang, M. Descour, T. Collier, M. Follen, A. Malpica, and R. Richards-Kortum, "Near real time *in vivo* fibre optic confocal microscopy: sub-cellular structure resolved," J. Microsc. **207**(2), 137–145 (2002).
11. P. M. Lane, S. Lam, and A. McWilliams, "J. C. IeRiche, M. W. Anderson, and C. E. MacAulay, "Confocal fluorescence microendoscopy of bronchial epithelium," J. Biomed. Opt. **14**(2), 02408 (2009).
12. H. Bertani, F. Pigò, E. Dabizzi, M. Frazzoni, V. G. Mirante, M. Manno, R. Manta, and R. Conigliaro, "Advances in endoscopic visualization of barrett's esophagus: the role of confocal laser endomicroscopy," Gastroenterol. Res. Pract. **2012**, 493961 (2012).

#179522 - $15.00 USD Received 8 Nov 2012; revised 10 Dec 2012; accepted 12 Dec 2012; published 18 Dec 2012

13. F. K. Shieh, H. Drumm, M. H. Nathanson, and P. A. Jamidar, "High-definition confocal endomicroscopy of the common bile duct," J. Clin. Gastroenterol. **46**(5), 401–406 (2012).
14. E. Coron, J. F. Mosnier, A. Ahluwalia, M. Le Rhun, J. P. Galmiche, A. S. Tarnawski, and T. Matysiak-Budnik, "Colonic mucosal biopsies obtained during confocal endomicroscopy are pre-stained with fluorescein *in vivo* and are suitable for histologic evaluation," Endoscopy **44**(02), 148–153 (2012).
15. S. E. Ilyin, M. C. Flynn, and C. R. Plata-Salamán, "Fiber-optic monitoring coupled with confocal microscopy for imaging gene expression *in vitro* and *in vivo*," J. Neurosci. Methods **108**(1), 91–96 (2001).
16. K. H. Al-Gubory and L.-M. Houdebine, "*In vivo* imaging of green fluorescent protein-expressing cells in transgenic animals using fibred confocal fluorescence microscopy," Eur. J. Cell Biol. **85**(8), 837–845 (2006).
17. V. Dubaj, A. Mazzolini, A. Wood, and M. Harris, "Optic fibre bundle contact imaging probe employing a laser scanning confocal microscope," J. Microsc. **207**(2), 108–117 (2002).
18. P. M. Lane, "Terminal reflections in fiber-optic image guides," Appl. Opt. **48**(30), 5802–5810 (2009).
19. W. H. Dzik and P. Szuflad, "Method for counting white cells (WBCs) in WBC-reduced red cell concentrates," Transfusion **33**(3), 272–273 (1993).
20. W. Göbel, J. N. D. Kerr, A. Nimmerjahn, and F. Helmchen, "Miniaturized two-photon microscope based on a flexible coherent fiber bundle and a gradient-index lens objective," Opt. Lett. **29**(21), 2521–2523 (2004).
21. X. Chen, K. L. Reichenbach, and C. Xu, "Experimental and theoretical analysis of core-to-core coupling on fiber bundle imaging," Opt. Express **16**(26), 21598–21607 (2008).
22. Y. Huang, K. Zhang, C. Lin, and J. U. Kang, "Motion compensated fiber-optic confocal microscope based on a common-path optical coherence tomography distance sensor," Opt. Eng. **50**(8), 083201 (2011).
23. S. F. Elahi, Z. Liu, K. E. Luker, R. S. Kwon, G. D. Luker, and T. D. Wang, "Longitudinal molecular imaging with single cell resolution of disseminated ovarian cancer in mice with a LED-based confocal microendoscope," Mol. Imaging Biol. **13**(6), 1157–1162 (2011).
24. T. J. Muldoon, N. Thekkek, D. Roblyer, D. Maru, N. Harpaz, J. Potack, S. Anandasabapathy, and R. Richards-Kortum, "Evaluation of quantitative image analysis criteria for the high-resolution microendoscopic detection of neoplasia in Barrett's esophagus," J. Biomed. Opt. **15**(2), 026027 (2010).

1. Introduction

Cervical cancer is the major form of cancer in females, both in developed and developing countries [1]. Cervical cancer therapy currently consists of surgery, radiation therapy, and chemotherapy. All have side effects and limitations [2]. A new therapeutic approach for cancer is gene therapy and it has been shown to be effective not only with cancer but also with many other types of diseases [3]. Cancer gene therapy can be defined as the delivery of gene(s) to cancer cells and has the following direct or indirect therapeutic effects: (1) self-destruct cancerous cells, (2) lower chance of recurrence, and (3) help increase the effectiveness of chemotherapy [4]. For successful gene expression, various gene delivery vectors including viruses and liposomes have been developed [5,6].

Among many methods that can measure how well various gene vectors are delivered and influence the target cells, the most common optical method is to detect tagged fluorescence signals from transfected cells using endogenous fluorescent probes such as green fluorescent protein (GFP) or cyan fluorescent protein (CFP) [7]. By comparing bright-field illumination and fluorescence images, gene transfection efficiency can be calculated as the ratio of fluorescence expressing cells to total cells. Fluorescence measurement and the assessment of the gene transfection efficiency of excised cancer tissue, however, are usually performed *in vitro* due to the limitation of accessibility in standard bench-top fluorescence microscopes. Therefore, to expand its imaging capability to the tissue in unperturbed physiological conditions, it is necessary to have an optical tool that enables *in vivo* imaging of cancer cells.

Recent advances in fiber-optic technologies have led to the development of several novel sub-cellular imaging methods *in vivo* [8]. A number of groups have developed flexible confocal endoscopes that can image *in vivo* based on high-resolution fiber bundles [9–11]. In addition, a commercial confocal microendoscope device (Cellvizio, France) that can acquire high-resolution real-time images of various tissues (e.g., esophagus, bile duct, and colon) via the instrument channel of an endoscope has been commercially available for several years [12–14]. Nevertheless, these systems function as either a confocal reflectance or a fluorescence microscope that makes it difficult to register both fluorescing and entire cells simultaneously. In this work, we propose a novel approach using a dual-modality microendoscope system that can simultaneously register both fluorescing and entire cells for

#179522 - $15.00 USD Received 8 Nov 2012; revised 10 Dec 2012; accepted 12 Dec 2012; published 18 Dec 2012

label-free optical assessment of intracellular gene delivery. The system uses two separate detection systems, enabling both high resolution reflectance and fluorescence imaging at the same time. The system automatically identifies and counts the cells from both images. As a result, gene transfection efficacy can be calculated by the ratio of cell counting from both images. There have been similar attempts to monitor gene expression in a rat brain [15], in extra-fetal membranes, and in the placenta of transgenic rabbits [16] using fiber-optic imaging techniques. These experiments clearly show that fiber-optic imaging—coupled with confocal microscopy for *in vitro* gene transfer studies—is practical, effective, and can also be applied to multiple organs *in vivo*. Prior studies, however, simply showed the feasibility of the concept as the studies focused on the fluorescent imaging, and the efficacy of the gene transfection was not considered or could not be assessed quantitatively.

We tested the system through *in vitro* studies using human cervical cancer cells (HeLa) with a non-viral CFP plasmid in four commercially available reagents and compared our results with that obtained using a conventional fluorescence microscope.

2. Materials and methods

2.1. System design

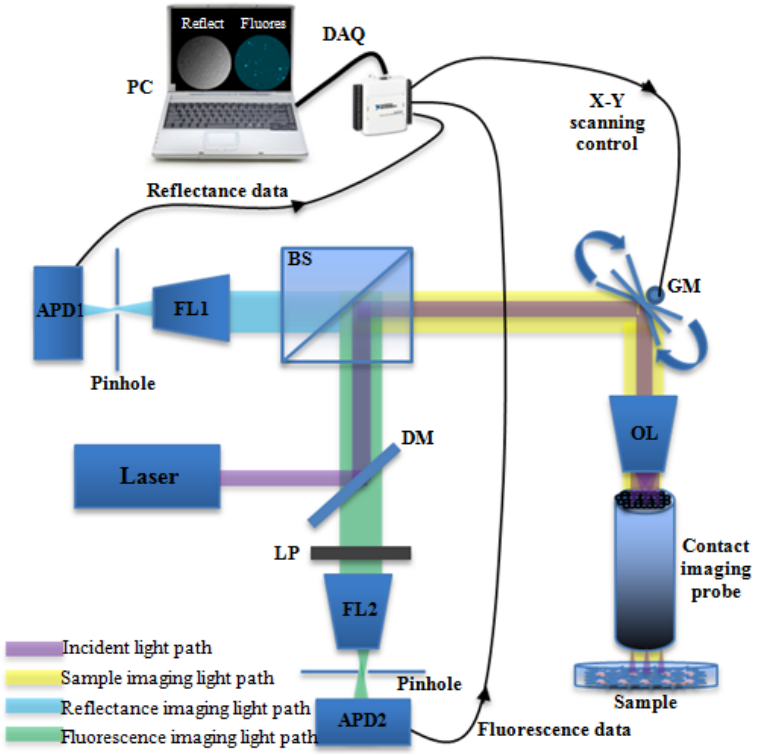

Fig. 1. System configuration (DM: dichroic mirror, BS: 50:50 beam splitter, GM: galvo mirror, OL: objective lens, FL 1&2: focusing lens, LP: longpass filter, APD 1&2: avalanche photodetector, DAQ: digital-to-analog & analog-to-digital converter).

A schematic of the imaging system is illustrated in Fig. 1. The laser scanning confocal microscope is connected to a coherent fiber bundle imaging probe [17]. Incident light from a 4-mW, 405-nm blue laser with beam dia. 3.0-mm x 5.0-mm (LDM 405, Thorlabs) is reflected by a dichroic mirror (DMLP425R, Thorlabs), a 50:50 beam splitter (BS013, Thorlabs), and an X-Y galvo scanner (GVS002, Thorlabs) in series and coupled into a multi-core fiber bundle by a microscope objective lens (Plan 20X/0.4, Olympus). The imaging probe is a coherent

#179522 - $15.00 USD Received 8 Nov 2012; revised 10 Dec 2012; accepted 12 Dec 2012; published 18 Dec 2012

fiber bundle (FIGH-10-500N, Fujikura) and consisted of 10,000 fiber cores with an image diameter of 460 μm. Returning light from the specimen is divided into two pathways by the beam splitter.

One pathway is used for the reflectance imaging (blue color in Fig. 1) which is directed through the beam splitter and spatially filtered using a focusing lens 1 (Plan N 10X/0.25, Olympus) and a 100-μm pinhole to reject background and out-of-focus light. APD 1 (APD110A, Thorlabs), highly sensitive Si avalanche photodiode, with an active area diameter of 1 mm2, is used to detect the reflectance imaging light.

The second pathway is used for the fluorescence imaging (green color in Fig. 1), which gets reflected by the beam splitter, transmitted through the dichroic mirror, and then filtered by a longpass filter (452 nm cut-off, Thorlabs) to obtain only the fluorescence signal. Similar to the reflectance imaging path, the longpass filtered beam is spatially filtered using a focusing lens 2 (Plan N 10X/0.25, Olympus) and a 100-μm pinhole. The resulting fluorescence signals are detected by APD 2 (APD110A2, Thorlabs), which is a UV-enhanced Si avalanche photodiode.

Data from two detectors are acquired simultaneously using a DAQ board (NI USB-6211, National Instruments) with a sampling rate of 250ks/s at 16-bit resolution (Fig. 2). Two analog output channels of the DAQ are used to control X-Y scanner mirrors. The graphical user interface, control software, and automated cell-counting algorithm are programmed using LabVIEW 2011 (National Instruments).

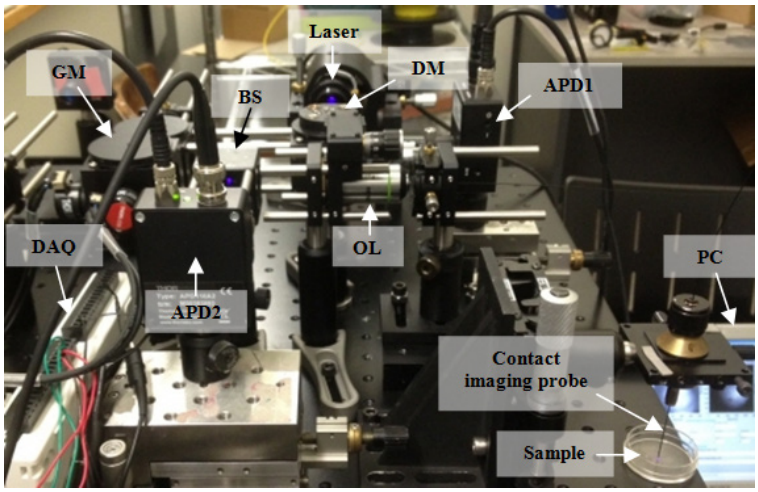

Fig. 2. Photograph of the system implementation.

2.2. Cell culture and preparation of transfection systems

HeLa cells were seeded onto 35-mm culture dishes (24 x 10^4 cells/ml) and allowed to adhere for 24 hours under standard tissue culture conditions the day before the transfection. The diluted 1.5-μg CFP plasmid DNA was mixed with 3.0 μl of four different transfection reagents (FuGENE 6, Lipofectamine 2000, Ultra, and X-tremeGENE HP) according to the manufacturer's instructions. Solutions were mixed and incubated for the appropriate time to allow formation of complexes. Finally, all the transfection complexes were transferred into the culture dish. All samples were fixed with 4% paraformaldehyde 24 hours after transfection.

2.3. Sample imaging and image analysis

We first used a U.S. Air Force resolution target to assess system resolution. The system has a maximum circular field of view 460 μm in diameter; the lateral resolution is approximately

#179522 - $15.00 USD Received 8 Nov 2012; revised 10 Dec 2012; accepted 12 Dec 2012; published 18 Dec 2012

3.5 μm (Fig. 3,) and images are displayed at 1 Hz with image size of 250 x 250 pixels. The image size and scanning rate limited by the hardware performance since the scanner has a maximum bandwidth of 250 Hz, but it could be further improved by replacement of the hardware that meets the requirement of high-rate scanning operations [10].

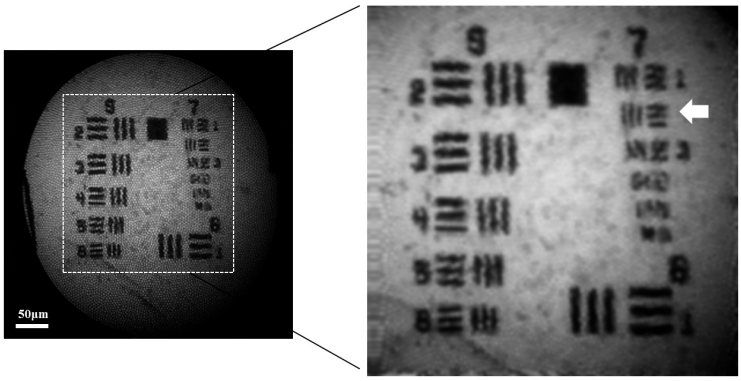

Fig. 3. USAF target image (raw data [left], processed data [right]; group 7 element 2– resolution 3.48 μm).

HeLa cell sample imaging in each of the reagent-induced transfection systems was conducted using both the presented system and a high-resolution bench-top fluorescence microscope (ECLIPSE TE2000-U, 20X/0.45, Nikon) for comparison. For the reflectance imaging of the microendoscope system, a reference image without the sample was used to subtract background due to the Fresnel reflection from the proximal end of the imaging probe [18]. The distal tip of the imaging probe was dipped into the culture dish and was nearly in contact with the sample. The 16-bit gray scale digital images were saved, processed, and analyzed. For each of the transfection systems, 5 images in different sites around the culture dish were taken randomly to count the average number of cells in the way that a conventional hemocytometer operates [19].

We implemented automated image analysis using MATLAB 2010a (MathWorks) to assess CFP expression in each of the transfection systems. The automated image processing algorithm performed the following procedures: (1) original data were contrast enhanced by histogram equalization; (2) spatial pixelation effects of the imaging probe were removed by applying Gaussian blurring (sigma equals to the core-to-core distance of 4.5 micron) [20]; (3) gray-thresholding was applied and the image went through an edge detector. Morphological operators of opening and closing, and labeling function provided by MATLAB is used to identify the spatial region correlated to cells. By labeling segmented cells, the total number of cells (T) is marked and counted and the number of fluorescence-expressing cells (F) is also counted from the images (see Fig. 4, Fig. 5). The ratio between the total and the number of fluorescence-expressing cells was used to determine how many cells were transfected by each of the vector systems.

2.4. Statistical analysis

Data were expressed as mean CFP expression percentages with standard error of 5 sites in different regions of the culture dish. One-way analysis of variance (ANOVA) was applied to determine the significance of differences among reagent groups; p values less than 0.05 were considered significant. For comparison of the results between the dual-modality microendoscope and the bench-top microscope, significance was determined by a Student's 2-sample t test, $p < 0.05$ (OriginPro 8, OriginLab).

#179522 - $15.00 USD Received 8 Nov 2012; revised 10 Dec 2012; accepted 12 Dec 2012; published 18 Dec 2012

3. Results

3.1. Dual-modality microendoscope sample imaging

Five random sites sample imaging in different transfection reagent groups were performed using our dual-modality microendoscope system. Representative imaging results are shown in Fig. 4. For the reflectance imaging, individual HeLa cells are distinguishable (Fig. 4(a)) and countable, as registered by the white X-marks in the middle of each cell (Fig. 4(b)). The negative control (untransfected cells) shows the largest cell population among groups; FuGENE 6 and X-tremeGENE HP have relatively high cell population, whereas Lipofectamine 2000 and Ultra have the lowest. In contrast, outer parts of the fluorescence imaging, control group displays no fluorescence signals compared to other reagents groups (Fig. 4(c)). The fluorescent cells appear blurred with flares due to the inter-core crosstalk between adjacent fibers [21] but can be segmented clearly. Fluorescent cells are also X-marked with red color and counted in the same way (Fig. 4(d)).

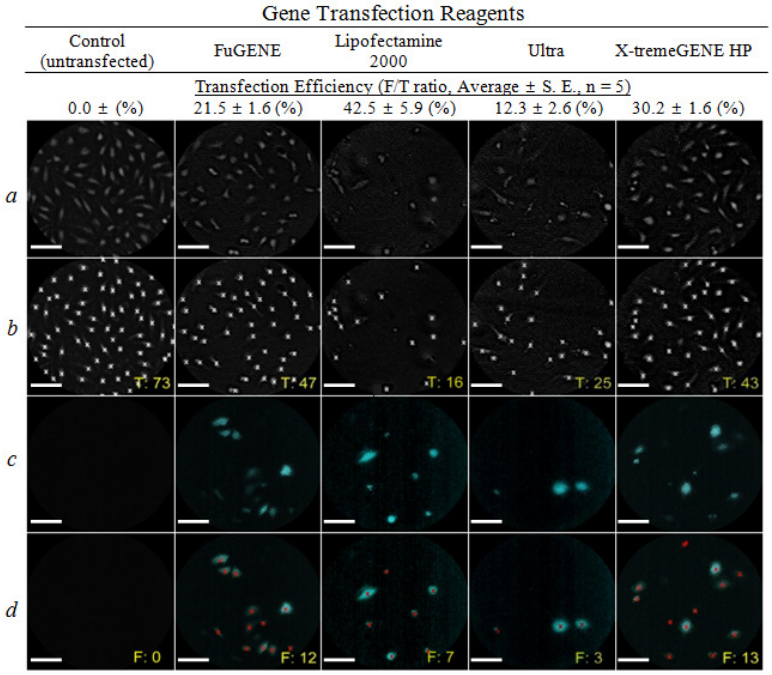

Fig. 4. Representative dual-modality microendoscope sample imaging results in four different reagent groups: *a*. reflectance image, *b*. total cell counting from the reflectance image, *c*. fluorescence image, d. fluorescent cell counting from the fluorescence image (All white bars – 100 μm, T: total cell counting number, F: fluorescent cell counting number, pseudo-color applied on the fluorescence images).

As represented in the top of Fig. 4, the Lipofectamine 2000 transfection reagent promoted maximal gene transfection efficiency (F/T ratio) in HeLa cells (42.5 ± 5.9%) compared to the other three reagents. X-tremeGENE HP resulted in the second highest (30.2 ± 1.6%). The difference in CFP expression between using Lipofectamine 2000 and X-tremeGENE HP was significant ($p < 0.05$). FuGENE 6 was third in CFP expression (21.5 ± 1.6%; $p < 0.05$), and Ultra contributed to the lowest gene transfection (12.3 ± 6.3%; $p < 0.05$).

3.2. Bench-top microscope imaging

For comparison, we also performed bench-top microscope imaging using the same samples. Figure 5 illustrates representative sample imaging results. In the bright-field imaging, not only

#179522 - $15.00 USD Received 8 Nov 2012; revised 10 Dec 2012; accepted 12 Dec 2012; published 18 Dec 2012

individual cells are visible, but the cell structures and even debris are also resolved (Fig. 5(a)). Images were automatically processed using the same MATLAB program and cells are segmented by green X-marks (Fig. 5(b)). As expected, the negative control group shows the largest population while the Lipofectamine 2000 and Ultra reagent groups have the least. For the fluorescent cells, cell shapes are clearly visible with no distortion or flares (Fig. 5(c)). Each cell is X-marked with red color (Fig. 5(d)).

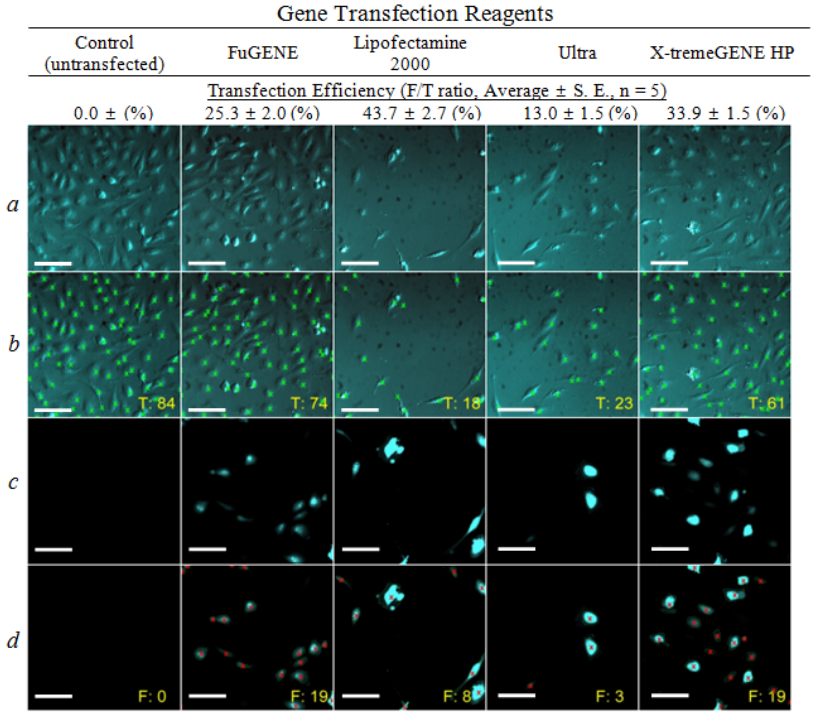

Fig. 5. Representative bench-top microscope sample imaging results in four different reagent groups: *a*. bright-field illumination image, *b*. total cell counting from the bright-field illumination image, *c*. fluorescence image, *d*. fluorescent cell counting from the fluorescence image (All white bars—100 μm, T: total cell counting number, F: fluorescent cell counting number, pseudo-color applied on fluorescence images).

Similarly, out of the four, the Lipofectamine 2000 transfection reagent promoted maximal transfection efficiency in HeLa Cells (43.7 ± 2.7%) compared to the other reagents (Fig. 5); X-tremeGENE HP resulted in the second highest CFP expression (33.9 ± 1.5%). The difference in CFP expression between using Lipofectamine 2000 and X-tremeGENE HP was significant ($p < 0.05$). FuGENE 6 was third in CFP expression (25.3 ± 2.0%; $p < 0.05$) and Ultra contributed to the lowest gene transfection (13.0 ± 1.5%; $p < 0.05$).

3.3. Comparison of the transfection efficiency results obtained by dual-modality microendoscopy and bench-top microscopy

A comparison of Fig. 4 and Fig. 5 showed that the cell-counting algorithm produced consistent results in both the dual-modality microendoscope and the bench-top microscope images. The average transfection efficiencies obtained with the dual-modality system tended to be lower than that obtained with the bench-top system. This result was observed because the imaging probe of the dual-modality microendoscope has a relatively smaller numerical aperture (NA, 0.39) than that of the bench-top system (NA, 0.45), thus lowering the fluorescence collection efficiency. However, the resultant relative efficacies of all four reagents observed using both imaging systems were found to be highly consistent. A statistical comparison of the two sets of images was done, and these results are illustrated in

#179522 - $15.00 USD Received 8 Nov 2012; revised 10 Dec 2012; accepted 12 Dec 2012; published 18 Dec 2012

Fig. 6. The bench-top microscope and the dual-modality microendoscope results were found to be clearly correlated, with the *p*-value being less than 0.05 by using the two-tailed Student's *t* test.

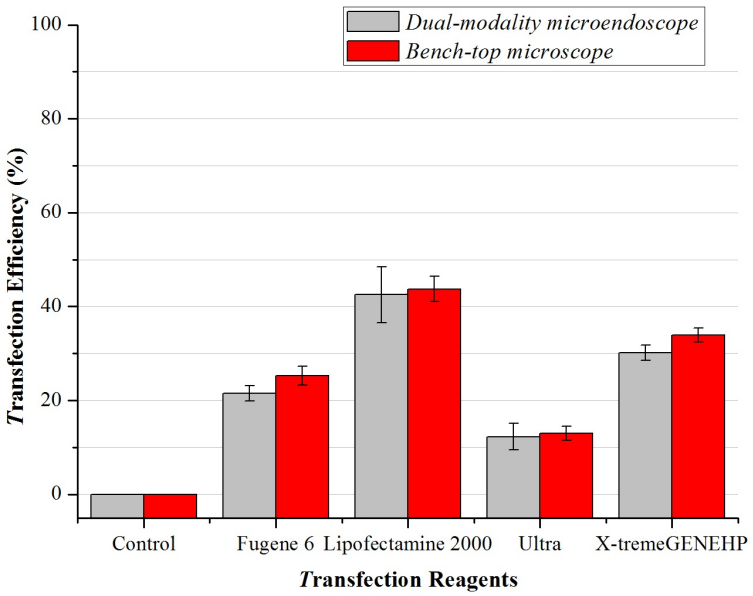

Fig. 6. Comparison of transfection efficiency in the four reagent groups

4. Discussion

Assessment of gene transfection efficacy in specific vector systems is essential in gene therapy studies. Optical imaging of gene transfection efficiency with flexibility, accessibility, and minimal invasiveness can be useful for evaluating the efficacy of gene therapy. Our dual-mode fluorescence microendoscope system has proved to be capable of measuring the gene transfection efficiency by simultaneously monitoring high-resolution reflectance and fluorescence images of HeLa cells. Albeit we utilized Gaussian degradation filter in the image-processing algorithm to remove the pixelation effects, individual cells were successfully identified and registered because of the sufficient signal-to-noise ratio accomplished by the imaging system.

In this study, we achieved approximately 3.5-μm lateral resolution, which was limited by the core size (2.9 μm) of the imaging bundle. This resolution proved the imaging performance to be adequate for obtaining individual cell imaging. Higher resolution, however, is still needed to achieve sub-cellular imaging. Once the CFP plasmid is transferred to the cell, significant amounts of CFPs are produced in the ribosome, and these proteins are seen regionally throughout the cells. As depicted in Fig. 5, the bench-top microscope resolved the micro-organelles (i.e., nuclei), which contributed to the fluorescence signals. However, our system was not able to resolve sub-cellular organelles. A coherent fiber bundle with a smaller core-to-core spacing and GRIN objective lens assembly at the distal end of the imaging probe will be implemented in the future to achieve higher resolution [11].

We are currently building an animal model for *in vivo* evaluation of our proposed approach. Although our pilot study is limited to preliminary validation of system performance for gene transfection efficiency *in vitro*, the same system can be employed for live animal studies. According to Lane et al. [11], it is still challenging to acquire high-quality images during *in vivo* imaging because of the movement of the imaging probe caused by motion artifacts such as heart beating and breathing in live animals. The imaging system can be

#179522 - $15.00 USD Received 8 Nov 2012; revised 10 Dec 2012; accepted 12 Dec 2012; published 18 Dec 2012

further improved by including motion artifact reduction by the motion compensation technique, which has recently been developed in our lab [22], and by increasing the imaging capability by using highly sensitive detectors and high-speed equipment for real-time assessment.

Another concern regarding *in vivo* imaging is that background reflections from tissues lower the contrast of cells, thereby preventing the accurate counting of the cell number. Recently, a study by Elahi et al. [23] on a rodent model with ovarian cancer showed that single cells expressing GFP fluorescence signals can be visualized by low excitation light power of 0.7 mW. They proved the feasibility of minimally invasive longitudinal imaging with single-cell resolution in live animals by using microendoscope technology. This result supports that our system is promising for a minimally invasive assessment of intracellular gene delivery *in vivo*. In addition, non-toxic agents such as acetic acid solution [10] and cresyl violet [11] can be used for contrast enhancing, which facilitates the identification and registration of cells both in reflectance and fluorescence modes. Furthermore, Muldoon et al. [24] proposed quantitative image analysis criteria for the detection of neoplasia in Barret's esophagus by extracting several features such as energy, nuclei per unit area, and mean nuclear separation distance. Similar approaches utilizing the characteristics of mean fluorescence intensity of the cell and mean cell size can also be applied to our image analysis, thus enhancing cell segmentation from the tissue effectively. These improvements will not only enhance image quality, but also make real-time assessment possible during *in vivo* imaging.

5. Conclusion

We have demonstrated the quantitative assessment of gene transfection efficacy by using a dual-modality microendoscope. The system is capable of simultaneously registering whole cells and fluorescence-expressing cells. *In vitro* imaging of HeLa cells expressing CFP demonstrates the system's ability to detect and resolve individual cells. Our study comparatively analyzed the gene transfection efficacy of four non-viral transfection systems targeting HeLa cells by using our dual-modality microendoscope system and a high-resolution bench-top fluorescence microscope. In both systems, individual cells were segmented and registered to obtain total cell and fluorescence-expressing cell counts. Statistical analysis of the experimental results showed that the gene transfection efficacy assessment using the dual-modality microendoscope is comparable to that using a bench-top microscope. The dual-modality microendoscope, however—unlike the bench-top microscope—can be used *in vivo*.

Acknowledgment

This work was supported by The Johns Hopkins Brain Science Institute.

#179522 - $15.00 USD Received 8 Nov 2012; revised 10 Dec 2012; accepted 12 Dec 2012; published 18 Dec 2012